

Formation of crystalline Si_9C_{15} nano-islands and Si_9C_{15}/graphene heterostructures on Ru(0001)

Lijing Huang(黄丽静), Yumeng Li(李雨萌), Hongqin Xiao(肖洪钦), Yuxuan He(何昱萱), Geng Li(李更), and Hong-Jun Gao(高鸿钧)

Citation: Chin. Phys. B, 2026, 35 (**5**): 056801. DOI: 10.1088/1674-1056/ae4c6f
http://cpb.iphy.ac.cn; http://iopscience.iop.org/cpb

What follows is a list of articles you may be interested in

Unchanged top surface-state structures in three-dimensional topological insulator Sb_2Te_3 thin films in the presence of bottom-surface moiré potentials

Dezhi Song(宋德志), Fuyang Huang(黄扶旸), Jun Zhang(仉君), and Ye-Ping Jiang(蒋烨平)
Chin. Phys. B, 2025, 34 (**12**): 126801. DOI: 10.1088/1674-1056/ae0926

Growth and characterization of Bi(110)/$CrTe_2$ heterostructures: Exploring interplay between magnetism and topology

Zhenyu Yuan(袁震宇), Fazhi Yang(杨发枝), Baiqing Lv(吕佰晴), Yaobo Huang(黄耀波), Tian Qian(钱天), Jinpeng Xu(徐金朋), and Hong Ding(丁洪)
Chin. Phys. B, 2024, 33 (**2**): 026802. DOI: 10.1088/1674-1056/ad082a

Visualizing interface states in In_2Se_3–WSe_2 monolayer lateral heterostructures

Da Huo(霍达), Yusong Bai(白玉松), Xiaoyu Lin(林笑宇), Jinghao Deng(邓京昊), Zemin Pan(潘泽敏), Chao Zhu(朱超), Chuansheng Liu(刘传胜), and Chendong Zhang(张晨栋)
Chin. Phys. B, 2023, 32 (**5**): 056803. DOI: 10.1088/1674-1056/acbaef

Molecular beam epitaxy growth of quantum devices

Ke He(何珂)
Chin. Phys. B, 2022, 31 (**12**): 126804. DOI: 10.1088/1674-1056/aca6d3

First principles study of hafnium intercalation between graphene and Ir(111) substrate

Hao Peng(彭浩), Xin Jin(金鑫), Yang Song(宋洋), and Shixuan Du(杜世萱)
Chin. Phys. B, 2022, 31 (**10**): 106801. DOI: 10.1088/1674-1056/ac6941

RAPID COMMUNICATION

Formation of crystalline Si_9C_{15} nano-islands and Si_9C_{15}/graphene heterostructures on Ru(0001)

Lijing Huang(黄丽静)[1,2,†], Yumeng Li(李雨萌)[1,2,†], Hongqin Xiao(肖洪钦)[1,2], Yuxuan He(何昱萱)[1,2], Geng Li(李更)[1,2,3,‡], and Hong-Jun Gao(高鸿钧)[1,2,3]

[1] *Beijing National Center for Condensed Matter Physics and Institute of Physics, Chinese Academy of Sciences, Beijing* 100190, *China*
[2] *School of Physical Sciences, University of Chinese Academy of Sciences, Beijing* 100190, *China*
[3] *Hefei National Laboratory, Hefei* 230088, *China*

(Received 16 January 2026; revised manuscript received 22 February 2026; accepted manuscript online 3 March 2026)

Two-dimensional silicon carbides have attracted increasing interest due to their highly tunable band structures and rich physical properties. Among them, Si_9C_{15} is particularly notable for its intrinsic auxeticity, strongly anisotropic carrier mobility, and pronounced optical and thermoelectric responses. However, the controlled growth of Si_9C_{15} nano-islands has remained a challenge. Here, we report a novel growth technique for Si_9C_{15} nano-islands. By exploiting the mild segregation of carbon atoms from a Ru(0001) substrate, we fabricate discrete, crystalline Si_9C_{15} nano-islands at temperatures as low as ~ 400 °C. Spectroscopic measurements reveal a spatial modulation of the local work function across the nano-island, which we attribute to the periodic potential landscape of the Si_9C_{15} lattice. Furthermore, we demonstrate that this island morphology enables the construction of Si_9C_{15}/graphene lateral heterostructures. Our work establishes a new pathway for fabricating Si_9C_{15} nanostructures as well as the heterostructures.

Keywords: Si_9C_{15}, nano-islands, low-temperature growth, heterostructure

PACS: 68.65.–k, 61.46.–w, 68.37.Ef, 73.22.–f

DOI: 10.1088/1674-1056/ae4c6f **CSTR:** 32038.14.CPB.ae4c6f

Two-dimensional (2D) silicon carbide materials have attracted growing interest due to their unique combination of carbon-based electronic characteristics and silicon compatibility,[1–5] making them promising candidates for next-generation electronic,[6,7] optoelectronic,[8,9] and energy-related devices.[10–14] The recent synthesis of Si_9C_{15} has brought new insights into this material family. Structurally, Si_9C_{15} can be regarded as a hybrid derivative of graphene[15] and silicene,[16,17] featuring a mixed hexagonal lattice composed of alternating Si–C and C–C rings.[18–20] Theoretical studies predict that Si_9C_{15} is a direct-bandgap semiconductor with a moderate, strain-tunable bandgap ($\sim$ 1.8–2.0 eV),[21,22] intrinsically auxetic and anisotropic properties,[19,21,23] as well as high and anisotropic carrier mobility that can be further enhanced via strain engineering and heterostructure design, rendering it promising for high-speed electronic and optoelectronic applications.[20,23,24] These results establish Si_9C_{15} as a versatile platform for multifunctional 2D heterostructure devices.

Despite the rapid progress in understanding its properties, the experimental realization of Si_9C_{15} has thus far been limited to continuous monolayers, with a gap size of 1.92 eV.[18] Compared with continuous films,[25–33] self-assembled nano-islands provide more efficient elastic strain relaxation,[17,34] better retention of coherent high-quality epitaxy,[35] and stronger size-dependent quantum-confinement control.[36] However, the controlled growth of Si_9C_{15} nano-islands remained unexplored. Furthermore, the existing synthesis technique is severely constrained by its requirement for extremely high temperatures to disrupt strong C–C bonding. In contrast, low-temperature growth has been successfully demonstrated for various other 2D materials.[37–39] Therefore, it is highly desirable to develop a new growth method that can produce Si_9C_{15} in the form of nano-islands under much milder thermal conditions.

Here, we present a new and versatile low-temperature growth technique for Si_9C_{15} nano-islands. Our approach utilizes the mild segregation of residual C atoms from a Ru(0001) substrate, allowing for the synthesis of Si_9C_{15} nano-islands at a temperature as low as ~ 400 °C and circumventing the need for high-energy C–C bond breaking. Furthermore, we demonstrate that the resulting morphology can be utilized to fabricate Si_9C_{15}/graphene lateral heterostructure.

We start by outlining the mechanism underlying our low-temperature synthesis of Si_9C_{15} nano-islands on Ru(0001). As schematically illustrated in Figs. 1(a) and 1(b), the Ru(0001) was annealed at ~ 400 °C to allow dissolved carbon atoms to migrate toward the surface via bulk-to-surface segregation.[40]

[†]These authors contributed equally to this work.
[‡]Corresponding author. E-mail: gengli.iop@iphy.ac.cn

© 2026 Chinese Physical Society and IOP Publishing Ltd. All rights, including for text and data mining, AI training, and similar technologies, are reserved.

Carbon has a finite solubility in Ru, and a small amount of residual carbon can remain in the near-surface region after standard sample preparation and thermal cycling. Upon annealing, thermally activated diffusion together with a thermodynamic driving force can promote surface precipitation, supplying a dilute population of discrete, non-bonded carbon species on Ru(0001) without formation of C–C bonds.[41] Subsequently, silicon atoms were deposited onto the Ru(0001) surface held at 400 °C using an electron-beam evaporator with a calibrated deposition rate of 0.33 monolayer/min (Fig. 1(c)). The locally segregated, highly reactive carbon atoms then directly participate in the surface reaction with incoming Si atoms, leading to the formation of Si–C bonds,[42,43] which subsequently evolve into discretely distributed Si_9C_{15} nano-islands and Si_9C_{15}/graphene heterostructures (Fig. 1(d)). Owing to the high chemical reactivity of the isolated carbon atoms, our pathway eliminates the need for high-temperature C–C bonds breaking, in sharp contrast to previously reported monolayer growth pathway[18,43–45] that require annealing at an extremely high temperature, around $\sim$ 1100 °C.

The scanning tunneling microscopy (STM) images were taken in a home-built STM system[46] with a base pressure below 2×10^{-10} mbar at the temperature of 4.2 K. The chamber was also equipped with low-energy electron diffraction (LEED) to verify the formation of ordered overlayers. STM measurements were performed in constant-current mode with an electrochemically etched tungsten tip, and all voltages were applied to the sample with respect to the tip. Scanning tunneling spectroscopy (STS) was carried out using a lock-in technique with a modulation amplitude of 20 mV at 861.3 Hz.

As shown in Fig. 2(a), the clean Ru(0001) substrate exhibits a hexagonal diffraction pattern, with distinct spots of Ru substrate indicated by the white arrows. Following low-temperature annealing and the Si dosing process, the LEED pattern changes dramatically (Fig. 2(b)). Additional diffraction spots appear (yellow arrow), forming a well-defined $\left(2\sqrt{3}\times2\sqrt{3}\right)R30^\circ$ super-structure with respect to the Ru spots. These features are characteristic of a highly ordered, rotationally-aligned Si_9C_{15} 2D crystal.

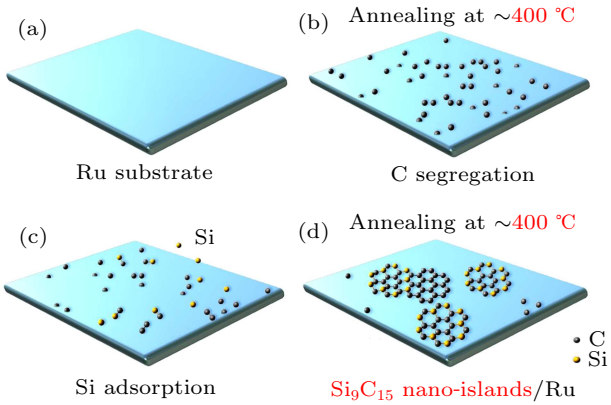


Fig. 1. Schematic of the low-temperature growth for crystalline Si_9C_{15} nano-islands and Si_9C_{15}/graphene heterostructures on Ru(0001) substrate. (a)–(d) Carbon atoms segregate from Ru bulk and react with deposited Si atoms to form Si_9C_{15} based nanostructures under low temperature of $\sim$ 400 °C.

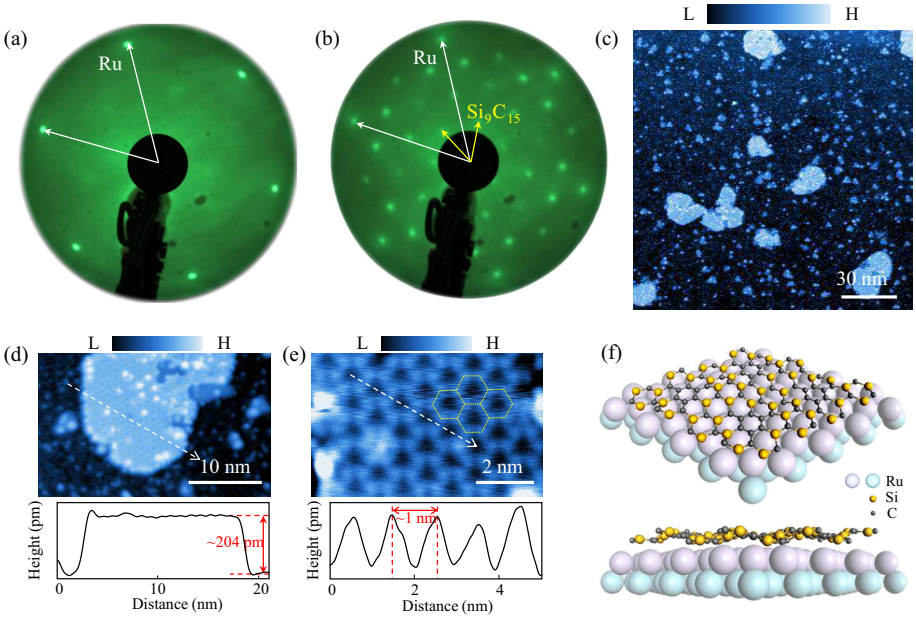


Fig. 2. Atomic structure of the Si_9C_{15} nano-islands confirmed by LEED and STM. (a) LEED pattern of the clean Ru(0001) substrate. The white arrows mark the diffraction spots of the Ru(0001) substrate. (b) LEED pattern after Si_9C_{15} nano-island growth. The yellow arrows mark the additional diffraction spots originating from the Si_9C_{15} overlayer. (c) Large-scale STM topography image showing the topography of the Si_9C_{15} nano-islands on the Ru(0001) surface ($V_s = -3$ V, $I_t = 50$ pA). (d) Zoomed-in STM image of an island from (c) ($V_s = -3$ V, $I_t = 50$ pA). The lower panel shows the height profile measured along the white dashed arrow in the upper panel. (e) Atomically-resolved STM image of the Si_9C_{15} nano-island ($V_s = -1$ V, $I_t = 200$ pA). The yellow dashed hexagons mark the characteristic honeycomb structure of the lattice. The lower panel shows the height profile measured along the white dashed arrow in the upper panel, showing a lattice constant of $\sim$ 1 nm. (f) Top and side views of the atomic model of Si_9C_{15}/Ru(0001).

A large-scale STM image (Fig. 2(c)) clearly reveals the existence of discretely distributed Si_9C_{15} nano-islands across the Ru surface. These islands exhibit a highly ordered internal structure, which collectively covers a significant portion of the surface. These nano-islands are characterized by smooth edges and a size of several tens of nanometers. A zoomed-in STM image (Fig. 2(d)) allows for precise determination of the layer thickness. The line profile (bottom panel in Fig. 2(d)) measured across an island indicates a uniform height of $\sim$ 200 pm, consistent with previous cross-sectional scanning transmission electron microscopy measurements of monolayer Si_9C_{15} on Ru.[18] The atomic resolution image (Fig. 2(e)) reveals the characteristic C_6 symmetry of the structure, marked by the yellow dashed hexagon. By measuring the distance between the periodically repeating units, we determine the lattice constant to be $\sim$ 1 nm (lower panel in Fig. 2(e)). Crucially, both the $\sim$ 1 nm periodicity observed in STM and the $\left(2\sqrt{3}\times2\sqrt{3}\right)R30^\circ$ super-structure identified in LEED are in excellent agreement with the proposed atomic model (Fig. 2(f)). In this model, the Si_9C_{15} lattice exhibits a periodicity $2\sqrt{3}$ times larger than that of the Ru substrate, accompanied by a 30° rotational alignment. This multi-scale correspondence between reciprocal-space LEED patterns and real-space STM images, both aligning perfectly with theoretical predictions, unambiguously confirms the successful growth of highly crystalline Si_9C_{15} nano-islands via our low-temperature segregation approach.

We then acquired STM images at different bias voltages to visualize the local density of states (LDOS) distribution across the unit cell at various energies (Figs. 3(a)–3(d)). The Si–C hexagonal ring regions maintain a consistently bright appearance in both the negative (Figs. 3(a) and 3(b)) and the positive (Figs. 3(c) and 3(d)) bias voltages. This suggests that the Si and neighboring C atoms contribute significantly to the LDOS across the Fermi level. In contrast, the C–C hexagonal ring regions appear dark at negative bias voltages, but dramatically brighten at positive bias voltages. This characteristic contrast reversal of the C–C hexagon centers is attributed to the inherent differences in the p-orbital contributions of the C atoms to the material's LDOS between the occupied and unoccupied states.[18,19]

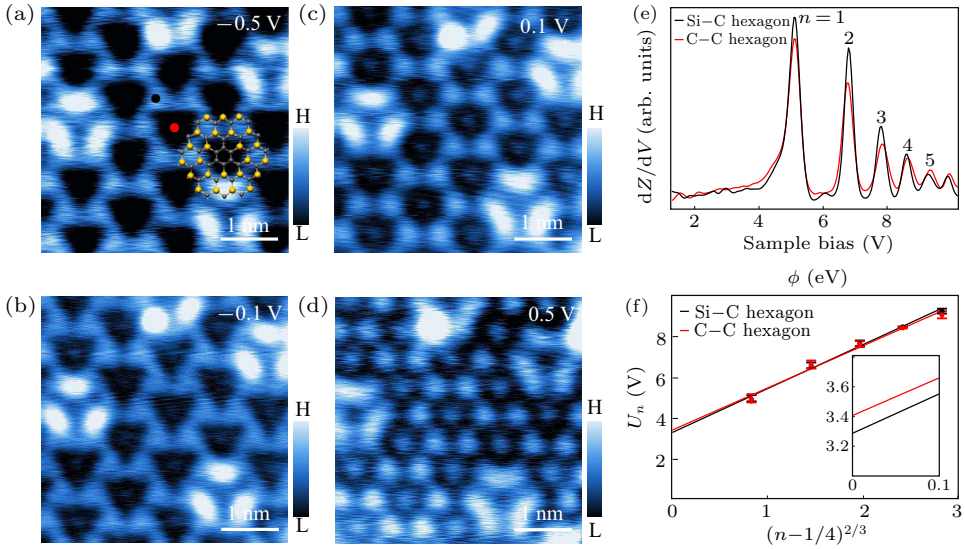


Fig. 3. Periodic modulation of local chemical potential in Si_9C_{15} nanoislands on Ru(0001). (a)–(d) Bias-dependent STM images of the Si_9C_{15} nano-island acquired at $V_s = -0.5$ V (a), -0.1 V (b), 0.1 V (c), and 0.5 V (d) ($I_t = 30$ pA). (e) Local dZ/dV spectra measured at the Si–C hexagon (black dot in (a)) and C–C hexagon (red dot in (a)). The shift in the spectral peak positions indicates local modulation in electronic properties. (f) Gundlach oscillation formula fitting analysis of the spectra in (e). The inset provides an enlarged view of the fitting intercepts, showing the different work function values between the Si–C and C–C hexagons.

Further localized measurement were conducted using dZ/dV spectroscopy (Fig.3(e), acquired from dots marked in Fig. 3(a)). The spectra obtained at the Si–C hexagon (black dot) and C–C hexagon ring region (red dot) show a measurable shift in the spectral peaks, which correspond to the energy positions of the field emission resonances.[47] This finding clearly demonstrates that the local electronic environment is not uniform across the nano-island, likely due to local interactions with the underlying Ru substrate. To quantify this difference, we performed an analysis utilizing the Gundlach oscillation[48] formula on the dZ/dV data (Fig. 3(f)), a highly established spectroscopic method for characterizing electron tunneling behavior and extracting local work function (Φ) values from STM data. The phenomenon of Gundlach oscillation arises from the quantum mechanical interference of the electron's wave function in the vacuum gap between the STM tip and the sample. The peak voltages (U_n) of these oscillations are related to the work function (Φ) and the quantum number (n) of the standing wave formed in the vacuum potential well.

This relationship can be linearized for fitting:[49]

$$U_n = \Phi + \left(\hbar^2/2m\right)^{1/3} (3\pi eF/2)^{2/3} (n-1/4)^{2/3},$$
$$n = 1,2,3,\ldots$$

Here, U_n is the voltage of the n-th peak, Φ is the work function, and F is the electric field. By plotting U_n against $(n-1/4)^{2/3}$ or a similar linearizing transformation, the resulting linear fit allows for the extraction of Φ. The intercept of this linear extrapolation directly corresponds to the value of the work function Φ.

The fitting confirms that a distinct work function difference exists between the Si–C and C–C hexagon regions, as evidenced by the different intercepts shown in the inset of Fig. 3(f). The work function at the C–C hexagon is ~ 0.1 eV higher than that at the Si–C hexagon. This variation in Φ is likely rooted in the islands' morphology, potentially linked to a local difference in the electrostatic dipole layer. Specifically, the periodic potential landscape created by the distinct C–C and Si–C hexagons, coupled with the local charge transfer at the Si_9C_{15}/Ru interface, may induce a spatially varying internal potential, thereby locally modulating the work function.

We further demonstrate the fabrication of a Si_9C_{15}/graphene lateral heterostructure using the new synthesis route. The process begins with the as-grown Si_9C_{15} islands (Fig. 4(a)). After annealing at 400 °C for 1 hour, the STM image (Fig. 4(b)) shows that mobile C atoms, segregated from the Ru bulk, begin to accumulate in the vicinity of the existing Si_9C_{15} islands. This suggests that the edges of the Si_9C_{15} islands serve as nucleation centers, facilitating the assembly of segregated carbon atoms into graphene nano-islands.

After further annealing for 2 hours, larger graphene nano-islands form, leading to the Si_9C_{15}/graphene lateral heterostructure (Fig. 4(c)). The image clearly shows the adjacent growth of Si_9C_{15} islands and newly formed graphene islands. A high-resolution STM image clearly reveals the interface of the lateral Si_9C_{15}/graphene heterostructure (Fig. 4(d)). The boundary between the Si_9C_{15} and graphene domains is marked by a white dashed line, indicating a seamless connection between the two materials. The heterostructure growth across the Ru surface is further confirmed by the LEED measurements. The LEED patterns of samples annealed for 1 hour (Fig. 4(e)) and 2 hours (Fig. 4(f)) exhibit diffraction spots from both Si_9C_{15} (yellow arrow) and the graphene spots (pink arrow). Notably, the graphene diffraction spots in Fig. 4(e) are less well ordered than those in Fig. 4(f), indicating increased sizes of graphene nano-islands with prolonged annealing. These observations confirm the macroscopic ordering of the Si_9C_{15}/graphene heterostructures. The formation of a lateral Si_9C_{15}/graphene heterostructure provides a clean in-plane junction between semiconducting and semi-metallic components, offering a versatile platform for future electronic devices and for exploring interfacial transport phenomena.

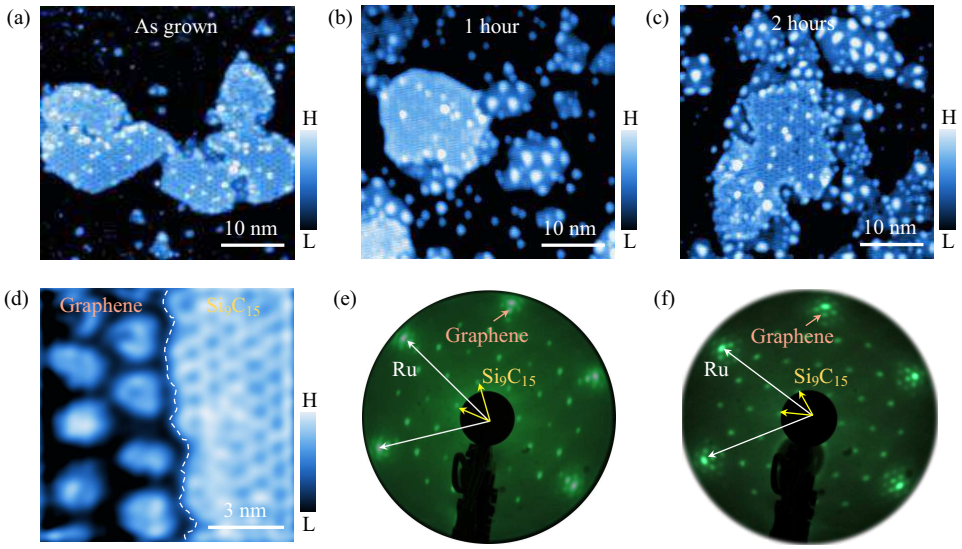


Fig. 4. Formation of Si_9C_{15}/graphene lateral heterostructure on Ru(0001) substrate. (a)–(c) STM images of the as-grown Si_9C_{15} nano-islands (a), sample after 1 hour annealing (b), and sample after 2 hours annealing (c) ($V_s = -3$ V, $I_t = 50$ pA). Graphene nano-islands form and grow during the extended annealing process. (d) STM image of the Si_9C_{15}/graphene boundary ($V_s = 1$ mV, $I_t = 50$ pA). The white dashed line indicates the boundary of the lateral heterostructure. (e) and (f) LEED results of the samples in (b) and (c), showing diffraction spots of the Ru substrate (white arrow), Si_9C_{15} (yellow arrow), and graphene (pink arrow). The graphene diffraction spots in (e) are less ordered than those in (f).

In summary, we have developed a novel synthesis route for Si_9C_{15} nano-islands, proceeding at a low temperature of ~ 400 °C. This innovative segregation-assisted method overcomes the high-temperature bottleneck of existing synthesis, enabling the controlled growth of Si_9C_{15} nano-islands. Spectroscopic measurements reveal spatial variations in the local work function across the islands, likely reflecting the periodic potential landscape of the Si_9C_{15} lattice. Furthermore, these nano-islands can assemble into ordered lateral heterostructures with graphene. Our results provide a significant advance in the

synthesis of Si_9C_{15} nano structures and open new opportunities for Si_9C_{15}-based planar devices.

Acknowledgements

The work is supported by the National Key Research and Development Project of China (Grant Nos. 2024YFA1207702 and 2022YFA1204100), the National Natural Science Foundation of China (Grant No. 62488201), the CAS Project for Young Scientists in Basic Research (Grant No. YSBR-003), and the Quantum Science and Technology-National Science and Technology Major Project (Grant No. 2021ZD0302700).

References

[1] Shi Z M, Zhang Z H, Kutana A and Yakobson B I 2015 *ACS Nano* **9** 9802
[2] Dong H L, Zhou L J, Frauenheim T, Hou T J, Lee S T and Li Y Y 2016 *Nanoscale* **8** 6994
[3] Dong H L, Wang L, Zhou L J, Hou T J and Li Y Y 2017 *Carbon* **113** 114
[4] Zheng F F, Dong H L, Ji Y J and Li Y Y 2019 *Appl. Surf. Sci.* **469** 316
[5] Zhou L J, Dong H L and Tretiak S 2020 *Nanoscale* **12** 4269
[6] Hsueh H, Guo G Y and Louie S G 2011 *Phys. Rev. B* **84** 085404
[7] Chen Y, Yu P F, Zhong Y M, Dong S K, Hou M X, Liu H L, Chen X, Gao J and Wong C P 2023 *ECS J. Solid State Sci. Technol.* **12** 045004
[8] Zhou L J, Zhang Y F and Wu L M 2013 *Nano Lett.* **13** 5431
[9] Liu X B, Shao X F, Yang B and Zhao M W 2018 *Nanoscale* **10** 2108
[10] Miró P, Audiffred M and Heine T 2014 *Chem. Soc. Rev.* **43** 6537
[11] Chabi S and Kadel K 2020 *Nanomaterials* **10** 2226
[12] Susi T, Skákalová V, Mittelberger A, Kotrusz P, Hulman M, Pennycook T J, Mangler C, Kotakoski J and Meyer J C 2017 *Sci. Rep.* **7** 4399
[13] Ding Y and Wang Y 2014 *J. Phys. Chem. C* **118** 4509
[14] Li Y F, Li F Y, Zhou Z and Chen Z F 2011 *J. Am. Chem. Soc.* **133** 900
[15] Novoselov K S, Geim A K, Morozov S V, Jiang D E, Zhang Y, Dubonos S V, Grigorieva I V and Firsov A A 2004 *Science* **306** 666
[16] Vogt P, De Padova P, Quaresima C, Avila J, Frantzeskakis E, Asensio M C, Resta A, Ealet B and Le Lay G 2012 *Phys. Rev. Lett.* **108** 155501
[17] Li G, Zhang L Z, Xu W Y, Pan J B, Song S R, Zhang Y, Zhou H T, Wang Y L, Bao L H and Zhang Y Y 2018 *Adv. Mater.* **30** 1804650
[18] Gao Z Y, Xu W P, Gao Y X, Guzman R, Guo H, Wang X Y, Zheng Q, Zhu Z L, Zhang Y Y and Lin X 2022 *Adv. Mater.* **34** 2204779
[19] Tagani M B 2023 *Phys. Rev. B* **107** 085114
[20] Xu Y H and Li D Q 2024 *Phys. Chem. Chem. Phys.* **26** 21789
[21] Zhou J L, Li J and Zhang J 2023 *Nanoscale* **15** 11714
[22] Zhai Z X, Guo H X, Zhang R Z, Li X H and Cui H L 2025 *Adv. Quantum Technol.* **9** e00803
[23] Jiang Y D, Zheng Y B, Qi S Y, Zhang M J, Wu L L, Zhao M W and Liu X B 2024 *Mater. Today Commun.* **40** 109905
[24] Cui Z, Lyu Y Y, Li R Y and Wu P F 2023 *Vacuum* **217** 112565
[25] Meng L, Wang Y L, Zhang L Z, Du S X, Wu R T, Li L F, Zhang Y, Li G, Zhou H T and Hofer W A 2013 *Nano Lett.* **13** 685
[26] Li L F, Wang Y L, Xie S Y, Li X B, Wang Y Q, Wu R T, Sun H B, Zhang S B and Gao H J 2013 *Nano Lett.* **13** 4671
[27] Li L F, Lu S Z, Pan J B, Qin Z H, Wang Y Q, Wang Y L, Cao G Y, Du S X and Gao H J 2014 *Adv. Mater.* **26** 4820
[28] Lin X, Lu J C, Shao Y, Zhang Y Y, Wu X, Pan J B, Gao L, Zhu S Y, Qian K, Zhang Y F, Bao D L, Li L F, Wang Y Q, Liu Z L, Sun J T, Lei T, Liu C, Wang J O, Ibrahim K, Leonard D N, Zhou W, Guo H M, Wang Y L, Du S X, Pantelides S T and Gao H J 2017 *Nat. Mater.* **16** 717
[29] Wu X, Shao Y, Liu H, Feng Z, Wang Y L, Sun J T, Liu C, Wang J O, Liu Z L, Zhu S Y, Wang Y Q, Du S X, Shi Y G, Ibrahim K and Gao H J 2017 *Adv. Mater.* **29** 1605407
[30] Li G, Zhang Y Y, Guo H, Huang L, Lu H L, Lin X, Wang Y L, Du S X and Gao H J 2018 *Chem. Soc. Rev.* **47** 6073
[31] Li E, Zhang R Z, Li H, Liu C, Li G, Wang J O, Qian T, Ding H, Zhang Y Y, Du S X, Lin X and Gao H J 2018 *Chin. Phys. B* **27** 086804
[32] Dong L, Wang A W, Li E, Wang Q, Li G, Huan Q and Gao H J 2019 *Chin. Phys. Lett.* **36** 028102
[33] Liu C, Li Z H, Qiao R X, Wang Q H, Zhang Z B, Liu F, Zhou Z Q, Shang N Z, Fang H W, Wang M X, Liu Z K, Feng Z, Cheng Y, Wu H, Gong D W, Liu S, Zhang Z S, Zou D X, Fu Y, He J, Hong H, Wu M H, Gao P, Tan P H, Wang X Q, Yu D P, Wang E G, Wang Z J and Liu K H 2022 *Nat. Mater.* **21** 1263
[34] Sautter K E, Schuck C F, Smith J C, Vallejo K D, Garrett T A, Soares J, Coleman H J, Henry M M, Jankowski E and Ratsch C 2021 *Cryst. Growth Des.* **21** 1674
[35] Gong Y J, Lin J H, Wang X L, Shi G, Lei S D, Lin Z, Zou X L, Ye G L, Vajtai R, Yakobson B I, Terrones H, Terrones M, Tay B K, Lou J, Pantelides S T, Liu Z, Zhou W and Ajayan P M 2014 *Nat. Mater.* **13** 1135
[36] García de Arquer F P, Talapin D V, Klimov V I, Arakawa Y, Bayer M and Sargent E H 2021 *Science* **373** eaaz8541
[37] Hoang A T, Hu L, Kim B J, Van T T N, Park K D, Jeong Y, Lee K, Ji S, Hong J and Katiyar A K 2023 *Nat. Nanotechnol.* **18** 1439
[38] Zhu J, Park J H, Vitale S A, Ge W J, Jung G S, Wang J, Mohamed M, Zhang T, Ashok M and Xue M 2023 *Nat. Nanotechnol.* **18** 456
[39] Gupta N, Singh B, Gautam S, Aggarwal V, Kumar R, Malik R and Kushvaha S S 2024 *Bull. Mater. Sci.* **47** 120
[40] McCarty K F, Feibelman P J, Loginova E and Bartelt N C 2009 *Carbon* **47** 1806
[41] Li G, Zhou H T, Pan L D, Zhang Y, Huang L, Xu W Y, Du S X, Ouyang M, Ferrari A C and Gao H J 2015 *J. Am. Chem. Soc.* **137** 7099
[42] Mao J H, Huang L, Pan Y, Gao M, He J F, Zhou H T, Guo H M, Tian Y, Zou Q, Zhang L Z, Zhang H G, Wang Y L, Du S X, Zhou X J, Castro Neto A H and Gao H J 2012 *Appl. Phys. Lett.* **100** 093101
[43] Guo H, Wang X Y, Huang L, Jin X, Yang Z Z, Zhou Z, Hu H, Zhang Y Y, Lu H L, Zhang Q H, Shen C M, Lin X, Gu L, Dai Q, Bao L H, Du S X, Hofer W, Pantelides S T and Gao H J 2020 *Nano Lett.* **20** 8584
[44] Pan Y, Zhang H G, Shi D X, Sun J T, Du S X, Liu F and Gao H J 2009 *Adv. Mater.* **21** 2777
[45] Pan Y, Shi D X and Gao H J 2007 *Chin. Phys.* **16** 3151
[46] Wu Z B, Gao Z Y, Chen X Y, Xing Y Q, Yang H, Li G, Ma R S, Wang A W, Yan J H and Shen C M 2018 *Rev. Sci. Instrum.* **89** 113705
[47] Zhang H G, Hu H, Pan Y, Mao J H, Gao M, Guo H M, Du S X, Greber T and Gao H J 2010 *J. Phys.: Condens. Matter* **22** 302001
[48] Gundlach K 1966 *Solid State Electron.* **9** 949
[49] Lin C L, Lu S M, Su W B, Shih H T, Wu B F, Yao Y D, Chang C S and Tsong T T 2007 *Phys. Rev. Lett.* **99** 216103